Two-Leg Deep-Space Relay Architectures: Performance, Challenges, and Perspectives

DARIO MODENINI , Member, IEEE
University of Bologna, Forlì, Italy

ALFREDO LOCARINI
University of Bologna, Forlì, Italy

LORENZO VALENTINI , Student Member, IEEE
ALBERTO FAEDI
University of Bologna, Cesena, Italy

PAOLO TORTORA , Senior Member, IEEE
University of Bologna, Forlì, Italy

DAVIDE ROVELLI
European Space Research and Technology Centre, Noordwijk, The Netherlands

NICOLÒ MAZZALI , Member, IEEE
European Space Research and Technology Centre, Noordwijk, The Netherlands

MARCO CHIANI , Fellow, IEEE
ENRICO PAOLINI , Senior Member, IEEE
University of Bologna, Cesena, Italy

In this article, architectures for interplanetary communications that feature the use of a data relay are investigated. In the considered

"two-leg" architecture, a spacecraft orbiting the Earth, or in orbit at a Lagrange point, receives data from a deep-space probe (leg-1) and relays them toward ground (leg-2). Different wireless technologies for the interplanetary link, namely, radio frequencies above the Ka band and optical frequencies, are considered. Moreover, the cases of transparent and regenerative relaying as well as different different orbital configurations are addressed, offering a thorough analysis of such systems from different viewpoints. Results show that, under certain constraints in terms of pointing accuracy and onboard antenna size, the adoption of a two-leg architecture can achieve the data rates supported by direct space-to-Earth link configurations with remarkably smaller ground station antennas.

I. INTRODUCTION

The use of extremely high radio frequency (RF) bands or optical frequencies in wireless digital communication systems is known to potentially allow achieving very high data rates, compared with the ones achievable at lower frequencies, for the same error rate performance. Such extremely high-frequency bands are, however, seldom employed in deep-space communication links due to their vulnerability to atmospheric impairments. They may, nevertheless, provide several advantages in deep-space telemetry (TM) and telecommand (TC) links in the framework of a "two-leg" relay architecture. Accordingly, a spacecraft (S/C) orbiting the Earth or in orbit at a Lagrange point would receive TM data from a deep-space probe and would relay them to the ground station (G/S). The deep space to relay link, not affected by the Earth atmosphere, may take advantage of an extremely high frequency band, e.g., frequencies between Ka-band ones and 75 GHz (which include the Q/V band), or the optical band, while the second link may use a more classical RF band, such as the K-band (for a near-Earth relay) or the X/Ka band (for a relay in a Lagrange point), benefiting from a shorter distance to the ground. The objective of this article is to provide a thorough analysis of two-leg deep-space architectures, with reference to TM links, assessing their potential advantages with respect to a classical direct link architecture. Emphasis is put on scenarios in which the deep-space probe is orbiting another planet of the solar system, so that the first link of the two-leg architecture, from the deep-space probe to the relay, is an interplanetary one.

Space data relaying has been attracting interest for a long time, being first envisaged by NASA in the late 60s [1]. More than a decade later, in 1983, the first tracking and data relay satellite service ever became operational, with the aim of providing near-continuous communications and tracking services to Low Earth Orbit (LEO) spacecrafts, launch vehicles, and suborbital platforms in general. Although several alternatives to offer data relay services to satellites orbiting in Earth proximity have been envisaged, mainly from national agencies, but also from commercial companies (e.g., [2], [3]), to date, only two successful relay satellite systems exist: 1) The Tracking and Data Relay Satellite System (TDRSS) and (2) The European Data Relay Satellite System (EDRSS) [4].

The reason behind considering LEO spacecrafts as the main use case for relay services lies in that, from a purely

coverage point of view, users getting the maximum benefit are spacecrafts orbiting below Geostationary Earth Orbit (GEO) altitude. On the other hand, since deep-space or planetary exploration missions can be tracked with a limited number of G/Ss in most situations, they have received less attention so far as potential users of relay constellations. Nonetheless, a few studies are available, mainly from NASA, assessing the feasibility of communication relay satellites in GEO orbit for deep-space users, operating whether at radio [5], or optical [6], frequencies. Recent studies involving relay satellites for deep space are primarily focused on optical links, [7]–[11], discussing performance requirements, candidate configurations, and future trends. The proposed concepts include an application of EDRS for data relaying with near-Earth and deep-space probes, called Data Relay for Moon (DROM), with possible extensions to Mars orbiters and next-generation NASA GEO optical relay satellites, aimed at offering data rates up to 2.88Gbps to lunar users and data rates in the order of 100Mbps to a deep-space mission to Psyche asteroid [10]. To the best of the authors' knowledge, however, none of the existing studies provides a systematic analysis of deep-space data relay systems encompassing, at the same time, different planetary targets, data relay orbital configurations, and frequency bands, a gap that this article aims to fill.

In this work, we investigate two-leg deep-space relay architectures with the goal of assessing their potential advantages over classical direct RF links for interplanetary communications. The analysis is carried out by considering 1) different wireless technologies for the interplanetary link, namely, radio frequencies above the Ka band and optical frequencies; 2) different relaying strategies, in particular transparent and regenerative relaying; and 3) different orbital configurations, including the relay position and the type of target (inner or outer planet). The number of degrees of freedom available to compare an architecture based on a direct link with a two-leg architecture is large and the problem may be tackled from several perspectives. Concerning link performance analysis, in this article, we take the following approach: We assume that the two-leg system shall support on both links the same data rate supported by the direct-link system, with the same error probability, and we investigate the benefits of the two-leg architecture in terms of ground antenna size. As a main outcome of this work, we show that in some cases, the ground antenna size can be considerably reduced, provided specific requirements in terms of S/C pointing accuracy and onboard antenna size can be met.

This article is organized as follows. Section II clarifies the notation used throughout the article and introduces preliminary elements such as the considered scenarios and the performance of direct links. In Section III, different alternatives for the orbit of the data relay S/C are discussed and compared. Section IV defines a framework for analysis of two-leg deep-space relay systems, including the case of transparent and regenerative relay, and addressing the problem of pointing losses and optical link analysis. Performance results are presented in Section V, while system engineering resources for an optical link are discussed in Section VI. Finally, Section VII concludes this article. A subset of the results, about pointing losses and optical link performance, appeared in the conference paper [12]. With respect to [12], this article includes results on orbital configurations, two-leg systems based on extremely high frequencies, as well as the system engineering resources analysis.

II. PRELIMINARIES AND NOTATION

A. Notation

When referring to a two-leg architecture, we use the subscript "1" to refer to the first link, i.e., the interplanetary link between the deep-space probe and the relay. This link is hereafter also referred to as "leg-1." Similarly, the subscript "2" refers to the second link, i.e., the one between the relay and the G/S. We often use the expression "leg-2" to refer to this second link. Then, for example, f_1 and f_2 denote the leg-1 and leg-2 carrier frequencies, respectively. With reference to any link (either from space to ground or from space to space), P_t and P_r denote the transmit and receive power, $G_t = G_t(f)$ and $G_r = G_r(f)$ the transmit and receive antenna gains, A_t and A_r the S/C transmit loss and the (G/S or S/C) receive implementation loss, and r the range (distance between the transmitter and the receiver), $A_{\mathrm{pnt},r}(f) = A_{\mathrm{pnt},r}$ and $A_{\mathrm{pnt},r}(f) = A_{\mathrm{pnt},r}$ the attenuation due to pointing mismatch. We also define the inverse of the pointing attenuation as $L_{\mathrm{pnt}} = 1/A_{\mathrm{pnt}}$ referred through the article as pointing loss. Concerning antennas, d_t and d_r denote the transmit and receive antenna sizes (i.e., diameters), while η_t and η_r are the corresponding efficiencies. For residual carrier modulation, the portion of the total received power apportioned to data is indicated as P_d. When analyzing a two-leg architecture where nonoptical frequencies are used in leg-1, we are mostly interested in values of f_1 belonging to the Q and V bands. For these frequencies, we often adopt the nomenclature extremely high frequencies (EHFs), although in principle, the EHF band is much wider, spanning from 30 to 300GHz.

Throughout the article, we denote by $A_{\mathrm{atm}} = A_{\mathrm{atm}}(f, \varphi, p)$ the atmospheric attenuation of a space-to-ground link, where f is the frequency, φ is the G/S antenna elevation angle, and p is the percentage of the time in which the link is unavailable. This latter parameter is directly related to the link availability: For example, $p = 5$ corresponds to 95% availability. In all cases, the atmospheric attenuation is computed as $A_{\mathrm{atm}} = A_{\mathrm{rain}} + A_{\mathrm{gas}} + A_{\mathrm{clouds}}$, i.e., by including attenuation caused by rain, absorption from gases (e.g., oxygen and water vapor), and small droplets (clouds and fog), according to International Telecommunication Union–Radiocommunication (ITU-R) recommendations, e.g., [13]–[15]. The atmospheric attenuation $A_{\mathrm{atm}}(f, \varphi, p)$ actually depends on a number of additional site-specific parameters at the G/S, which include the height above mean sea level, the point rainfall rate for 0.01% of an average year, the atmospheric pressure, the temperature,

TABLE I
Reference Scenarios for Missions to Venus, Mars, Uranus, and Neptune

Central body	Tx–Rx distance	Downlink band	Downlink Tx power	S/C antenna size
Venus	259,594,256 km (1.735280 AU)	X-band / Ka-band	65 W / 120 W	1.3 m / 2.5 m
Mars	400,373,069 km (2.676328 AU)	X-band	65 W	2.2 m
Uranus	3,155,452,867 km (21.092899 AU)	X-band	65 W	3 m
Neptune	4,687,074,599 km (31.331158 AU)	X-band / Ka-band	65 W / 100 W	3 m

the water vapour density, and the total columnar content of liquid water reduced to a temperature of 273.15K. All of these parameters have been estimated for the location of European Space Agency (ESA) deep-space antenna (DSA) 1, located in New Norcia, Australia, using the data made available by ITU-R. We also acknowledge that, following ESA Alphasat mission [16], data from several propagation experiments between Alphasat's Aldo Paraboni payload and different ground stations in Europe are made available in the literature, covering two frequencies at Ka and Q bands (19.7 and 39.4GHz, respectively) [17]–[20]. These experiments report in general fairly good agreement with ITU-R models, although with different levels of matching. Since, to the best of authors' knowledge, a new model based on the abovementioned experiments has not yet been consolidated, in this work, the choice has been made to stick to the current ITU-R models for atmospheric attenuation computation.

When analyzing the mutual geometry between the deep-space probe, the Sun, and the data relay S/C, the first will be referred as the "probe," identified with the letter "P," and the last will be identified with the letter "D," so that the angular separation between the Sun "S" vector and the transmitter–receiver line of sight will be denoted as Sun - data relay - deep space probe (SDP) angle or Sun - deep space probe - data relay (SPD) angle depending on whether we are considering the field of view (FOV) of the data relay spacecraft or that of the deep-space probe, respectively.

Finally, throughout the whole article, we denote by B_r the data rate, i.e., the information bit rate at the input of the channel encoder. The energy per information bit is E_b while the one-sided noise power spectral density is $N_0 = kT_{\text{syst}}$, where $k = 1.38 \times 10^{-23}$ J/K is the Boltzmann constant and T_{syst} is the receiver system noise temperature expressed in Kelvin.

B. Reference Scenarios

Deep-space missions targeting a selection of inner (Venus) and outer (Mars, Uranus, and Neptune) solar system planets are considered to establish some reference application cases. Emphasis is put, whenever possible, to the most recent missions, which are more representative of the state-of-the-art. For each central body considered as a possible target, a relevant scenario was derived for a classical direct space-to-Earth link, based on data from the surveyed missions involving orbiting spacecraft (i.e., excluding fly-by only ones). The key parameters adopted

to characterize the deep-space direct communication link are transmitter–receiver maximum distance, downlink frequency band, transmit power, and antenna size. The reference scenarios for Venus, Mars, Uranus, and Neptune are reported in Table I. Note that the range values reported in the table correspond to the worst-case range.

C. Performance of Classical Direct Links

The performance of a classical direct (one-leg) space-to-Earth link can be evaluated through a standard link budget procedure. Specifically, we have

$$\frac{P_r}{N_0} = \frac{P_t G_t G_r}{A_t A_r A_{\text{atm}} A_{\text{pnt},t} A_{\text{pnt},r} k T_{\text{syst}}} \frac{c^2}{(4\pi f r)^2} \quad (1)$$

where c is the light speed, and the meaning of the other parameters involved in the expression has been clarified in Section II-A. Moreover, the portion of the total received power apportioned to data, P_d, fulfills

$$P_d/N_0 = \begin{cases} P_r/N_0 & \text{suppressed carrier modulation} \\ P_r/N_0 \sin^2(\beta) & \text{residual carrier modulation} \end{cases} \quad (2)$$

where β is the modulation index (for residual carrier modulation). Recommended residual carrier modulation types are PCM/PSK/PM and PCM/PM/Bi-ϕ [21], [22]. The available E_b/N_0 at the G/S is

$$\frac{E_b}{N_0} = \frac{P_d}{N_0 B_r} \quad (3)$$

where, as mentioned above, B_r is the data rate. The E_b/N_0 margin can be computed as the difference between the available E_b/N_0 (3) and the parameter $(E_b/N_0)^*$, referred to as the required E_b/N_0 and representing the minimum E_b/N_0 value to achieve the target bit error rate (BER) or frame error rate (FER). The value of $(E_b/N_0)^*$ depends on the employed coding and modulation.

Table II summarizes the achievable data rate values in the four considered scenarios for a direct X-band link at maximum range. These values have been obtained via standard link budget assuming the parameters reported in Table I, and targeting ESA DSA-1, characterized by $d_r = 35$m and $G/T_{\text{syst}} = 50.1$dB [23], [24]. The transmit antenna efficiency and the transmit and receive losses are set to $\eta_t = 0.7$, $A_t = 1.5$dB, and $A_r = 0.5$dB in all scenarios. The X-band atmospheric attenuation, computed for 95% availability and $\varphi = 10°$ elevation angle (commonly employed values for the X-band), turns to be $A_{\text{atm}} = 0.5$dB,

while pointing losses turn to be negligible. In compliance with recommendations, the modulation schemes are residual carrier ones while the employed channel coding schemes are the rate-1/4 (28560,7136) turbo code for Venus and Mars and the rate-1/6 (42840,7136) turbo code for Uranus and Neptune. The E_b/N_0 margin is 4dB in all cases.

III. TWO-LEG SYSTEM ORBITAL CONFIGURATIONS

We consider different two-leg orbital geometries, assuming the relay to be placed whether on LEO, GEO or at a lagrangian point of the Earth–Sun system, and the deep-space probe orbiting at an inner or outer planet. The resulting configurations are compared according to their complexity, occultation/conjunction time, and range. The typical distance between the relay S/C and an hypothetical ground station, involved in each scenario, is included in Table III.

A. Relay Spacecraft in LEO

The exploitation of the near-Earth space for data relay to support deep-space missions provides some advantages in terms of reduction of the orbital deployment costs, as they would benefit of the wide offer of launches targeting LEO heights. Moreover, a LEO data buffer enables the possibility to use any of the numerous small stations commonly employed in near-Earth missions, spread at a very wide range of latitudes and longitudes.

However, to guarantee an adequate geometric visibility between the relay and the deep-space probe, which may be requested to be nearly 100% during the most critical mission phases, multiple LEO relays would be required. As an additional drawback, a deep-space observer would experience an angular separation between the Earth and the relay spacecraft so small that the Earth would act as a continuous source of noise for an hypothetical optical receiver.

B. Relay Spacecraft in GEO

Most of the advantages and disadvantages for a LEO relay S/C apply also to the GEO scenario, the main difference being the drastic reduction of Earth occultation at the geosynchronous distance. Although the range between the transmitter and the receiver in leg-2 is larger than for the LEO case, it still allows using smaller stations than the ones employed in deep-space missions, with the additional benefit of a simpler ground segment architecture, by selecting a station which is always in view of the GEO satellite. On the other hand, the space segment architecture would result more complex than for the LEO case, because of the need for an onboard propulsion system for orbit deployment and maintenance.

C. Relay Spacecraft in a Lagrange Point

L4 and L5 (equilateral) Lagrange points are the more promising candidates for data relay, being the only stable among the five equilibrium points of the Sun–Earth system. They are placed on the same trajectory covered by the Earth around the Sun, preceding and following the Earth, respectively, with a phase difference of approximately $60°$. L1/L2 Lagrange points are also considered, despite the additional complexity resulting from the expected increased station-keeping effort make them less attractive. Although placing a relay on L4 or L5 leads to the highest range (1AU) for leg-2, the high angular separation from the Earth would allow for a favorable observation geometry from both inner and outer planets, when either the Earth or the L4 (or L5) point is in solar conjunction with the target.

D. Geometric Visibility Analysis

The relative geometry between the Sun, the relay S/C, and the target planet will affect the percentage of link outage due to the possible presence of the Sun in (or close to) the line-of-sight between the transmitter and the receiver. This is especially true when an optical link is chosen for leg-1, as Sun radiation is by far the largest noise source which would affect such a link. To this end, an analysis has been performed which, starting from the mutual orbital configurations, predicts the temporal evolution of the SDP/SPD angles for each planetary target of interest over the next 100 years. Fig. 1 depicts the SDP and SPD geometries for the cases of a mission to both an inner and an outer planet.

We compute the link outage percentage as the amount of time, over the total mission lifetime, at which the SDP/SPD angle is below a certain value, resulting in the impossibility to establish the link. Since such a threshold is (optical) hardware dependent, the comparison among different configurations should include computation of 1) the outage percentage corresponding to different cut-off values of SDP/SPD angles, and 2) the minimum SDP/SPD angle that the optical instrument shall be capable to operate at, for an assumed percentage of link availability loss (a value of 10% was adopted for this work).

In the framework of the SDP/SPD analysis, a data relay S/C placed at the Lagrange points L4 and L5 or in LEO/GEO
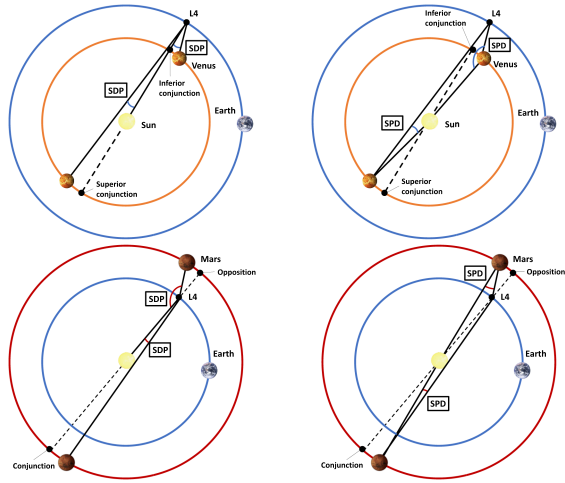
Fig. 1. Graphical visualization of the SDP and SPD angles for a deep-space probe to inner and outer planets.

TABLE IV
Outage Percentage Assuming SDP Thresholds Equal to 1°, 3°, 10°, and 40°

Outage SDP	Venus	Mars	Uranus	Neptune
40°	69.67%	35.92%	23.41%	23.37%
10°	14.95%	9.08%	5.85%	5.82%
3°	3.84%	2.65%	1.76%	1.63%
1°	0.25%	0.48%	0.45%	0.23%

TABLE V
Outage Percentage Assuming SPD Thresholds Equal to 1°, 3°, 10°, and 40°

Outage SPD	Venus	Mars	Uranus	Neptune
40°	37.75%	87.27%	100%	100%
10°	9.55%	16.89%	100%	100%
3°	2.55%	4.64%	94.45%	100%
1°	0.53%	1.24%	21.95%	35.04%

TABLE VI
Min SDP Associated to Link Availability Loss of 10%

	Venus	Mars	Uranus	Neptune
Outage SDP	7.1°	11.0°	17.0°	17.1°
Outage SPD	10.46°	6.01°	0.46°	0.30°

TABLE VII
Min SDP/SPD Angles Achievable With a Combined L5 + Earth Communication Architecture

	Venus	Mars	Uranus	Neptune
Min SDP L5+Earth	12.39°	17.51°	28.55°	29.08°
Min SPD L5+Earth	17.33°	11.19°	1.37°	0.92°

displays the value of the minimum SDP and SPD angles that the data relay and deep-space probe communication equipment, respectively, must be able to operate with when considering a maximum loss of link availability due to the solar noise of 10%. Results indicate that, at Venus (Mars), the optical equipment must be designed to operate with SDP/SPD values down to 7.1° (11°) for the relay S/C and 10.6° (6.01°) for the deep-space probe. Deep-space probes at Uranus and Neptune must instead cope with more severe optical design requirements in terms of straylight rejection capabilities and narrower FOV, since lower SPD values are involved.

A relay S/C in L4/L5 would benefit from a larger angular separation from the Earth. Table VII shows the minimum values of SDP/SPD, which result from assuming to switch between an optical communication to the L4/L5 relay and a direct RF link with Earth depending on which of the two geometries is more advantageous when approaching conjunction. When either L4 or L5 is at low SDP angles, ground-based deep-space antennas on the Earth may be used to send telecommands to the probe. The same consideration applies also for the data downlink from a deep-space probe at Venus and Mars, while at Uranus or Neptune, the SPD would still be very low even considering the alternative direct link to the Earth. To be noted that such an advantage may only be exploited under the assumption that the deep-space probe is equipped with a redundant telecommunication segment, one optical and one RF segment, as optical link is not considered a suitable solution for direct communication with Earth, because of its high sensitivity to the atmospheric conditions.

IV. TWO-LEG SYSTEM LINK ANALYSIS FRAMEWORK

Following the existing literature, e.g., [25], [26], we distinguish between the two cases of transparent relay and regenerative one. A transparent relay performs signal amplification and carrier frequency conversion, without attempting any signal demodulation and channel-decoding operation. Conversely, a regenerative relay demodulates and decodes the signal incoming from the spacecraft, re-encodes, and remodulates the data, and retransmits them to the G/S, possibly using a carrier frequency different from the one of the received signal. In case of a transparent relay, the employed coding and modulation scheme is the same in both legs; in contrast, regenerative relays allow using different coding and modulation options and also different wireless technologies, e.g., optical and RF, for the two legs, but require data-buffering capabilities. A general end-to-end signal-to-noise ratio (SNR) analysis of a multihop

orbit around the Earth are treated as a single scenario, as they all move within the same orbital plane and at the same distance from the Sun. This means that the "relay–Sun" vector presents the same temporal evolution (with a phase offset) for any of the L4, L5, or Earth orbiting scenario, i.e., the same SDP/SPD dynamics. Since placing a relay in L1/L2 results to only slight differences in the numerical values with respect to the L4/L5/LEO/GEO case, no explicit distinction will be made when presenting the data, for the sake of brevity.

Results are illustrated by means of tables. Tables IV and V display the outage percentages for the cases when SDP (or SPD) is lower than 1°, 3°, 10°, and 40°. Moreover, Table VI

communication system based on transparent relaying was developed in [27].

A. Transparent Relay

We consider the case in which RF signals are transmitted both links (hence, no optical technology is used). The signal power received by the relay in leg-1 is given by

$$P_{r,1} = \frac{P_{t,1}G_{t,1}G_{r,1}}{A_{t,1}A_{r,1}A_{\mathrm{pnt},t,1}A_{\mathrm{pnt},r,1}} \frac{c^2}{\left(4\pi f_1 r_1\right)^2} \quad (4)$$

where we note the absence of atmospheric attenuation due to the relay being out of the Earth atmosphere. Denoting by $B_{\mathrm{eq},1}$ the equivalent noise bandwidth of the receiver onboard the relay, the thermal noise power impairing the signal received in leg-1 is $N_1 = N_{0,1}B_{\mathrm{eq},1} = kT_{\mathrm{syst},1}B_{\mathrm{eq},1}$. The SNR at the relay is therefore $\mathsf{SNR}_1 = P_{r,1}/N_1$. Since both signal and noise are amplified and forwarded by the relay, the power transmitted by the relay in leg-2 may be expressed as

$$P_{t,2} = P_{t,2}^{(s)} + P_{t,2}^{(n)} \quad (5)$$

where $P_{t,2}^{(s)}$ is the amplified signal power and $P_{t,2}^{(n)}$ is the amplified noise power. Letting $P_{r,2}$ be the total power received on ground, contributed by both the signal and the noise forwarded by relay, the SNR at the G/S may, therefore, be expressed as

$$\mathsf{SNR}_2 = \frac{P_{r,2}^{(s)}}{P_{r,2}^{(n)} + N_2} = \frac{P_{r,2}\frac{P_{r,1}}{P_{r,1}+N_1}}{P_{r,2}\frac{N_1}{P_{r,1}+N_1} + N_2} \quad (6)$$

in which $N_2 = N_{0,2}B_{\mathrm{eq},2} = kT_{\mathrm{syst},2}B_{\mathrm{eq},2}$. Simple algebraic manipulation yields

$$(\mathsf{SNR}_2)^{-1} = \frac{N_1}{P_{r,1}} + \frac{N_2}{P_{r,2}}\left(1 + \frac{N_1}{P_{r,1}}\right) \quad (7)$$

where

$$\frac{N_1}{P_{r,1}} = \frac{A_{t,1}A_{r,1}A_{\mathrm{pnt},t,1}A_{\mathrm{pnt},r,1}N_1}{P_{t,1}G_{t,1}G_{r,1}} \frac{\left(4\pi f_1 r_1\right)^2}{c^2} \quad (8)$$

and

$$\frac{N_2}{P_{r,2}} = \frac{A_{t,2}A_{r,2}A_{\mathrm{pnt},t,2}A_{\mathrm{pnt},r,2}A_{\mathrm{atm},2}N_2}{P_{t,2}G_{t,2}G_{r,2}} \frac{\left(4\pi f_2 r_2\right)^2}{c^2}. \quad (9)$$

Next, we define an equivalent one-sided noise power spectral density N_0 as

$$N_0 = \frac{P_{r,2}^{(n)} + N_2}{B_{\mathrm{eq},2}} \quad (10)$$

which allows us writing

$$\frac{P_{r,2}^{(s)}}{N_0} = \mathsf{SNR}_2 B_{\mathrm{eq},2} = \left[\frac{N_1}{P_{r,1}} + \frac{N_2}{P_{r,2}}\left(1 + \frac{N_1}{P_{r,1}}\right)\right]^{-1} B_{\mathrm{eq},2}. \quad (11)$$

The results presented in Section V about two-leg relay systems with a transparent relay will mainly rely on the parameter $P_{r,2}^{(s)}/N_0$.

B. Regenerative Relay

In the regenerative case, we do not impose use of RF signals in leg-1, which may be either an EHF or an optical link. Leg-2, instead, is assumed to be an RF link. Denoting by E_1 and E_2 the decoding error events in the relay and in the G/S, respectively, we have an error in the two-leg regenerative configuration when an E_2 event occurs. We can develop the error probability as

$$\begin{aligned}\Pr\left(E_2\right) &= \Pr\left(E_2|E_1\right)\Pr\left(E_1\right) + \Pr\left(E_2|\bar{E}_1\right)\Pr\left(\bar{E}_1\right) \\ &= \Pr\left(E_2|E_1\right)\Pr\left(E_1\right) + \Pr\left(E_2|\bar{E}_1\right)\left(1 - \Pr(E_1)\right).\end{aligned} \quad (12)$$

In the last row of (12), $\Pr(E_2|E_1)$ is the probability to have a decoding error in the G/S given that an error in the relay occurred. This probability is essentially 1. Moreover, since the link budget in both links is designed to have small error probabilities (e.g., decoding error probability in the order of 10^{-4}), we have $1 - \Pr(E_1) \approx 1$. We then obtain, with very good approximation,

$$\Pr\left(E_2\right) \approx \Pr\left(E_1\right) + \Pr\left(E_2|\bar{E}_1\right) = P_{\mathrm{e},1} + P_{\mathrm{e},2} \quad (13)$$

where $P_{\mathrm{e},1} = \Pr\left(E_1\right)$ and $P_{\mathrm{e},2} = \Pr\left(E_2|\bar{E}_1\right)$. Equation (13) tells us that, in case of a regenerative relay, we can analyze the two links separately and design them under a constraint in the form

$$P_{\mathrm{e},1} + P_{\mathrm{e},2} \leq P_{\mathrm{e}}^* \quad (14)$$

where P_{e}^* is the maximum tolerable decoding error probability.

C. Pointing Losses

The extremely narrow optical beams pose very tight requirements in terms of pointing accuracy. In fact, the mispointing losses between the transmit and the receive antennas cannot be neglected even in presence of a very accurate point-ahead calculation, due to mechanical noise generated by the vibrations and the satellite motions [28]. Moreover, despite the wider beam of RF systems, EHF links can also be affected by nonnegligible pointing losses. This can be due, for example, to a lower accuracy of the RF antenna pointing systems.

Most available studies on pointing effects assume that only one antenna is affected by angular errors [29]. For example, when one edge of the communication link is on ground, a very precise ground pointing can be assumed and, therefore, it is usual to consider the angular noise only on the S/C. In case of space-to-space links (such as leg-1 in a two-leg system), however, pointing effects should be carefully considered at both edges of the link. In the following we propose an approach to address the mispointing losses in situations where both terminals are affected by angular noise. In addition, we introduce the concept of *effective system gain* to optimize the antenna gain capturing pointing accuracy.

Pointing in a three-dimensional space is affected by both azimuth and elevation angular errors. Considering these two errors are independent and identically distributed (i.i.d.) and

Gaussian distributed with zero-mean, the resulting random angular error θ (i.e., the angle between the line of sight and the pointing direction) is Rayleigh distributed as [28], [30]

$$f_\theta(\theta) = \frac{\theta}{\sigma_\theta^2} e^{-\theta^2/(2\sigma_\theta^2)}, \quad \theta \geq 0 \tag{15}$$

where σ_θ is the main angular noise parameter, hereafter referred to as the *pointing accuracy*. We also need to assume a pointing loss model for both the receiver and the transmitter. For example, the Gaussian beam point loss model is given by [28]

$$L_{pnt}(\theta) = e^{-G\theta^2} \tag{16}$$

where $L_{pnt} = 1/A_{pnt}$ is the inverse of the pointing attenuation referred through the article as pointing loss, G is the linear-scale antenna gain, and θ is the angular mispointing error. Another model is the circular aperture one where the pointing losses are instead given by [28], [31]

$$L_{pnt}(\theta) = \left(\frac{2 J_1 \left(\sqrt{G}\theta \right)}{\sqrt{G}\theta} \right)^2 \tag{17}$$

where $J_1(\cdot)$ is the Bessel function of the first kind of order 1.

We may use two approaches to include pointing losses in the link analysis. The first one is a deterministic approach which considers a maximum angular error θ_{max} (based on the available information about the pointing system). Using this value, it is possible to quantify the loss by employing, for example, (16) or (17) model. Adopting a Gaussian beam model, for given θ_{max} we compute the maximum pointing loss per antenna as

$$L_{pnt,max} = e^{-G\theta_{max}^2} \tag{18}$$

and we use it for link analysis.

We may also adopt a probabilistic approach. Accordingly, we define the outage probability as

$$P_{out} = \mathbb{P}\left\{ A_{pnt,t}[dB] + A_{pnt,r}[dB] > A_{pnt}^*[dB] \right\} \tag{19}$$

where $A_{pnt}[dB] = -L_{pnt}[dB]$ is the pointing attenuation, the subscripts "t" and "r" refer to the transmitter and the receiver, respectively, and $A_{pnt}^*[dB]$ is the margin against the pointing attenuation. For given P_{out}, $A_{pnt}^*[dB]$ represents the value of pointing attenuation to be included in the link budget. Under a Gaussian beam model and an angular error distribution (15), we can derive P_{out} in closed form as

$$P_{out} = \frac{G_t \sigma_{\theta,t}^2 e^{-K/(2\sigma_{\theta,t}^2 G_t)}}{G_t \sigma_{\theta,t}^2 - G_r \sigma_{\theta,r}^2} + \frac{G_r \sigma_{\theta,r}^2 e^{-K/(2\sigma_{\theta,r}^2 G_r)}}{G_r \sigma_{\theta,r}^2 - G_t \sigma_{\theta,t}^2} \tag{20}$$

where $K = \frac{\ln(10)}{10} A_{pnt}^*[dB]$. Considering a symmetrical system where $G_t = G_r = G$ and $\sigma_{\theta,t} = \sigma_{\theta,r} = \sigma_\theta$, the outage probability becomes

$$P_{out} = \left(1 + \frac{K}{2\sigma_\theta^2 G} \right) e^{-K/(2\sigma_\theta^2 G)}. \tag{21}$$

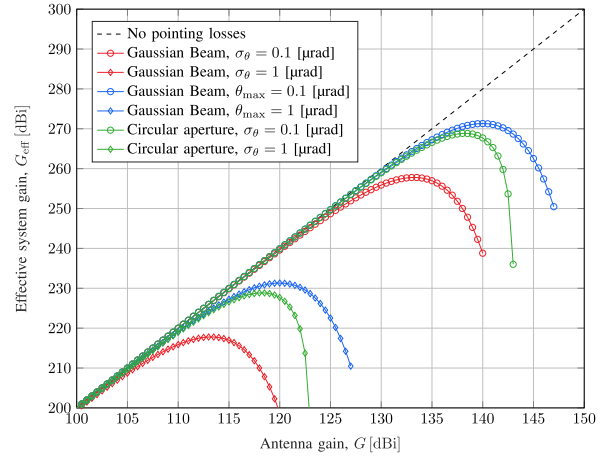Fig. 2. Effective system gain (23) versus the antenna gain $G = G_t = G_r$. Deterministic (θ_{max}-based) and probabilistic (σ_θ-based) approaches; $P_{out} = 5\%$ when probabilistic approach is employed; different values of the pointing accuracy parameters; Gaussian beam and circular aperture models.

Different beam models or angular error distributions may require numerical evaluation.

Regardless of the approach used to estimate the pointing losses and the adopted model, we can define an "effective system gain" as

$$G_{eff} = \left(G_t L_{pnt,t} \right) \left(G_r L_{pnt,r} \right) \tag{22}$$

i.e., as the product of the transmit and receive antenna gains, each multiplied by the corresponding pointing loss. Looking at the effective system gain reveals the existence of an optimal value for the antenna gains, beyond which the overall system performance degrades instead of improving. Considering a situation where the transmitter and the receiver are equipped with the same antennas, the effective system gain assumes the form

$$G_{eff}[dBi] = 2G[dBi] - A_{pnt,tot}[dB] \tag{23}$$

where $A_{pnt,tot}[dB]$ incorporates the total pointing attenuation. Sticking for simplicity to the case in which both antennas exhibit the same pointing accuracy parameter σ_θ or θ_{max}, we can numerically find $A_{pnt,tot}[dB]$ (and therefore $G_{eff}[dBi]$) for any given gain $G[dBi]$, for a particular value of P_{out} and σ_θ (or θ_{max} if the deterministic approach is adopted). An example is shown in Fig. 2 for different values of the pointing accuracy parameter σ_θ or θ_{max} depending on the approach employed, different pointing loss models (Gaussian beam or circular aperture), and the outage probability $P_{out} = 5\%$ for the probabilistic approach.

D. Optical Link Analysis

To date, the only coding and modulation scheme recommended for deep-space optical telemetry is represented by serially concatenated pulse position modulation (SCPPM) [32]. For peak and average power constraints typical of a deep-space link, restricting the modulation to pulse position modulation (PPM) is near-capacity achieving. The SCPPM scheme is reviewed in Appendix A, along

with some performance curves obtained via Monte–Carlo simulation. Hereafter, we target use of SCPPM in leg-1, when optical frequencies are used.

For the analysis of optical links, we resort on optical link budget techniques [33], [34], together with the above-introduced effective system gain G_{eff}. Denote by P_e^* the maximum tolerable value of decoding error probability, by n_s the actual received signal photon flux, expressed in dB phe/ns, and by n_s^* the minimum such number required to satisfy the $P_e \leq P_e^*$ requirement for a given coding and modulation scheme. The optical path loss attenuation, $A_{opt} = A_{opt}(\lambda, r)$, is given by $A_{opt} = ((4\pi r)/\lambda)^2$, where r is the range and λ the wavelength. Moreover, the transmit and receive optical antenna gains can be computed, similarly to the RF case,[1] as

$$G_t = ((\pi D_t)/\lambda)^2 \quad \text{and} \quad G_r = ((\pi D_r)/\lambda)^2 \quad (24)$$

respectively. For given P_{out} and σ_θ (probabilistic approach) or given θ_{max} (deterministic approach), we can compute the antenna gains and the corresponding pointing losses, to maximize the effective system gain G_{eff}. This is done by tuning the antenna diameter if λ is fixed. In the following, we assume both G_t and G_r take their optimum values in terms of G_{eff} optimization.

The number of received signal photons n_s may be expressed as

$$n_s = \text{EIRP} G_r \eta_r \frac{\lambda}{hc} A_{opt}^{-1} \quad (25)$$

where the equivalent isotropically radiated power (EIRP) is given by

$$\text{EIRP} = P_{ave} G_t \eta_t L_{pnt} L_{extra} \quad (26)$$

and where η_t and η_r are the efficiencies of the transmit and receive antennas, respectively. The parameter L_{extra} includes possible extra losses. Letting $n_{s,margin}$ be the link margin, the difference $n_s^*[\text{dBphe/ns}] = n_s[\text{dBphe/ns}] - n_{s,margin}[\text{dBphe/ns}]$ represents the value of the number of received signal photons for which, for given average number of background noise photons n_b, the SCPPM scheme must guarantee the target performance over the considered channel, e.g., Poisson PPM if photon counting detection is used [35]. A suitable combination of the SCPPM parameters M, T_s, and code rate R (see Appendix A) can then be found to fulfill the constraints, yielding the achieved data rate B_r. Denoting by N_1 the number of cyclic redundancy check (CRC) and termination bits and by T_F the time duration of the coded PPM channel block, we have

$$B_r = \frac{15120R - N_1}{T_F} = \frac{15120R - N_1}{MT_s(15120/\log_2 M)\alpha_{GT}} \quad (27)$$

where the factor $\alpha_{GT} > 1$ captures the guard times. For instance, with a 25% guard time (with respect to the coded PPM block time), we have $\alpha_{GT} = 1.25$.

---

[1]Conventionally, at optical frequencies, antenna efficiencies are not incorporated in the gain.

Estimation of the background noise is performed by computing the noise photons per second, n_b, through

$$n_b = \frac{P_{source}}{hf} \quad (28)$$

where P_{source} is the optical noise power generated by the considered noise source (sun, planet, star), h the Plank's constant, and f the radiation frequency. Values of P_{source} have been estimated using the ITU-R approach provided in [36]. The Sun direct noise is found to be several orders of magnitude greater than that from other sources. For this reason, we assume that no optical communication can be established between the two S/Cs when any portion of the Sun is in the FOV of the receiver. When the instrument is free of the Sun direct noise, the only considered noise contribution is the solar radiation reflected from the central body of the deep-space probe orbit as a function of its albedo. This, in turn, is computed assuming the planet fully illuminated and entirely contained within the instrument FOV (worst-case).

V. RESULTS

This section is devoted to the analysis of the performance of two-leg deep-space relay systems, along with comparison with systems based on a direct X-band link (Section II-C). In particular, Section V-A addresses the case of a transparent relay, while the case of a regenerative relay is considered in Section V-B, including both EHF and optical bands in leg-1.

A. Results for Transparent Relay

In the transparent relay case, we use the framework discussed in Section IV-A, with the goal of investigating the range of values of the leg-1 frequency f_1 for which the two-leg configuration can outperform the direct one, for the same input values (the ones summarized in Table I, including the transmit power of the deep-space probe), the same G/S (35m DSA), and for a leg-2 frequency $f_2 = 27\text{GHz}$. The value $f_2 = 27\text{GHz}$ belongs to the recommended range for near-Earth space-to-Earth communication [21]. A GEO relay is considered.

The pointing losses have been estimated through the method based on θ_{max}. The values of the system noise temperature in the relay and in the G/S have been set to $T_{syst,1} = T_{syst,2} = 100\text{K}$. Finally, the atmospheric attenuation at 27GHz, assuming the DSA-1 location (New Norcia), has been computed using the ITU-R recommendations; the obtained value is 1.33dB for 95% availability with an elevation angle $\theta = 53.89°$, corresponding to a GEO relay. The results have been obtained for an EIRP of the GEO relay equal to 62dBW. It should be remarked, however, that the results exhibit a very low sensitivity to the relay EIRP, since the two-leg system performance is limited essentially by the first link.

Fig. 3 shows the G/S P_r/N_0 value of the direct X-band link and the G/S $P_{r,2}^{(s)}/N_0$ values of the two-leg system, given by the right hand side of (11), for a link availability of 95%
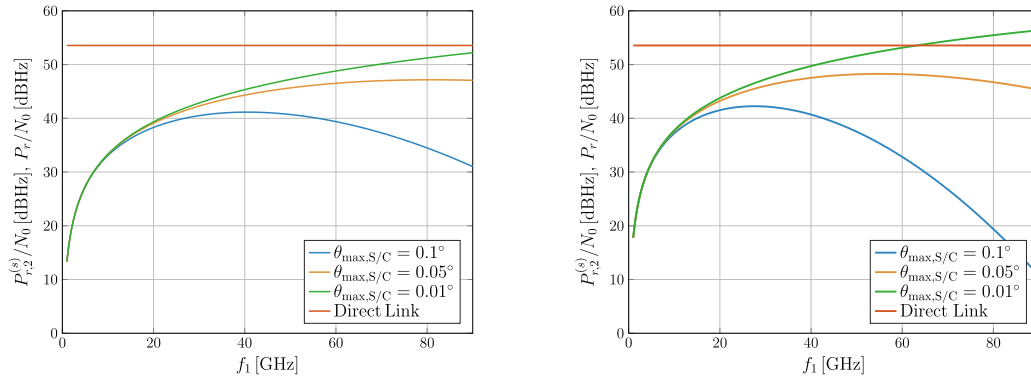
Fig. 3. $P_{r,2}^{(s)}/N_0$ values of a two-leg system with transparent relay versus the leg-1 frequency f_1, compared with the P_r/N_0 value of a direct link X-band system (red horizontal line); 95% availability, relay receive antenna diameter $d_{r,1} = 3$m (left), and $d_{r,1} = 5$m (right), several pointing error values. Mars scenario.

and for a relay receive antenna diameter $d_{r,1}$ of 3 and 5m, respectively. The two parameters are plotted versus the leg-1 frequency f_1 (hence the direct link P_r/N_0 remains constant). In both figures, curves for the two-leg system are shown for values of the maximum pointing error $\theta_{\max} = 0.1°$, $\theta_{\max} = 0.05°$, and $\theta_{\max} = 0.01°$ in the S/Cs (deep-space probe and relay, both in transmission and reception), while $\theta_{\max} = 10^{-4}$rad $\approx 0.0057°$ has been assumed in all cases at the G/S. The considered scenario is Mars, but very similar results are obtained in the other cases.

The P_r/N_0 of the direct link remains essentially the same for all maximum pointing error values, owing to the use of the X-band. As it is possible to observe, when the relay antenna diameter equals 3m, the $P_{r,2}^{(s)}/N_0$ values for the two-leg system are lower than the ones of the direct X-band link for all values of f_1 in the range of interest, and regardless of the pointing errors. For a relay receive antenna diameter of 5m and only for a spacecraft maximum pointing error of $\theta_{\max} = 0.01°$, the two-leg system exhibits some gain over the direct link one. More in detail, for $f_1 \approx 63$GHz, the $P_{r,2}^{(s)}/N_0$ values of the two-leg system matches the P_r/N_0 value of the direct link system. In this situation, if the two systems use the same coding and modulation, they achieve the same data rate B_r with the same reliability. For frequencies f_1 larger than this value, the two-leg system exhibits a gain that may be used to decrease the ground antenna size for the same data rate. We observe, however, that the gain is marginal so that the transparent configuration seems not a viable solution. More encouraging results have been found for regenerative relays, as addressed in the following.

B. Results for Regenerative Relay

As pointed out in Section IV-B, in the regenerative case, we can analyze the two links separately. We start with the analysis of leg-2, showing that this link is not critical for the considered data rate. We then focus on leg-1, including both the EHF and the optical case.

1) *Leg-2 Analysis:* We provide an analysis of leg-2 (relay-to-ground link) considering three different relay options, namely, a GEO relay, a relay placed in Lagrange point L1, and a relay placed in Lagrange points L4/L5. We

assume a relay transmit power $P_{t,2} = 65$W, transmit antenna diameter $d_{t,2} = 2$m, efficiency $\eta_{t,2} = 0.7$, and transmit implementation loss $A_{t,2} = 1.5$dB, corresponding to an EIRP of approximately 70dBW at 27GHz. The receiver system noise temperature is set to $T_{\text{syst}} = 100$K. Atmospheric losses are computed for a percentage of link availability equal to 95% and 10° elevation in all cases. Pointing losses are computed using the deterministic model, assuming maximum pointing errors $\theta_{\max,\text{G/S}} = 100\mu$rad $\approx 0.0057°$ at the G/S and $\theta_{\max} = 0.05°$ at the relay.

Fig. 4 illustrates the available E_b/N_0 in each of the scenarios of interest. With suppressed carrier modulation, the available E_b/N_0 can be computed as the ratio of P_r/N_0 (the same for all scenarios) to the data rate B_r. To this aim, we use the data rate values shown in Table II (X-band direct link data rates) and summarized hereafter: 100kbps (Venus), 120kbps (Mars), 3.15kbps (Uranus), and 1.2kbps (Neptune). Blue curves in Fig. 4 are relevant to a GEO relay, orange curves to an L1 relay, and green curves to an L4/L5 relay. Moreover, solid, dashed, and dot-dashed curves correspond to a G/S antenna diameter of 35, 15, and 2.4m, respectively.

Assuming $(E_b/N_0)^* = 4$dB, corresponding to a concatenated scheme employing a punctured (7, 3/4) convolutional code and a (255,223) RS code with interleaving depth 16, and an E_b/N_0 margin of 4dB, the available E_b/N_0 at the G/S should be at least 8dB. As we can observe looking at Fig. 4, this is not a concern for a GEO or a Lagrange L1 relay, regardless of the G/S antenna size, in the whole f_2 frequency range, apart from frequencies around 60GHz. The large observed margins are due to the low data rates since, as explained previously, we are targeting the same data rate in both legs.

As Lagrange L4/L5 points are in deep space, in case of a Lagrange L4/L5 relay a frequency f_2 in X-band or Ka-band should be considered. Using as channel coding scheme the rate-1/4 turbo code with information block length 7136 bits, the minimum E_b/N_0 to achieve a target BER of 10^{-6} is $(E_b/N_0)^* = 0.23$dB, so we need at least 4.23 dB to achieve an E_b/N_0 margin of 4dB. As we can see from Fig. 4, in the Uranus and Neptune scenarios use of
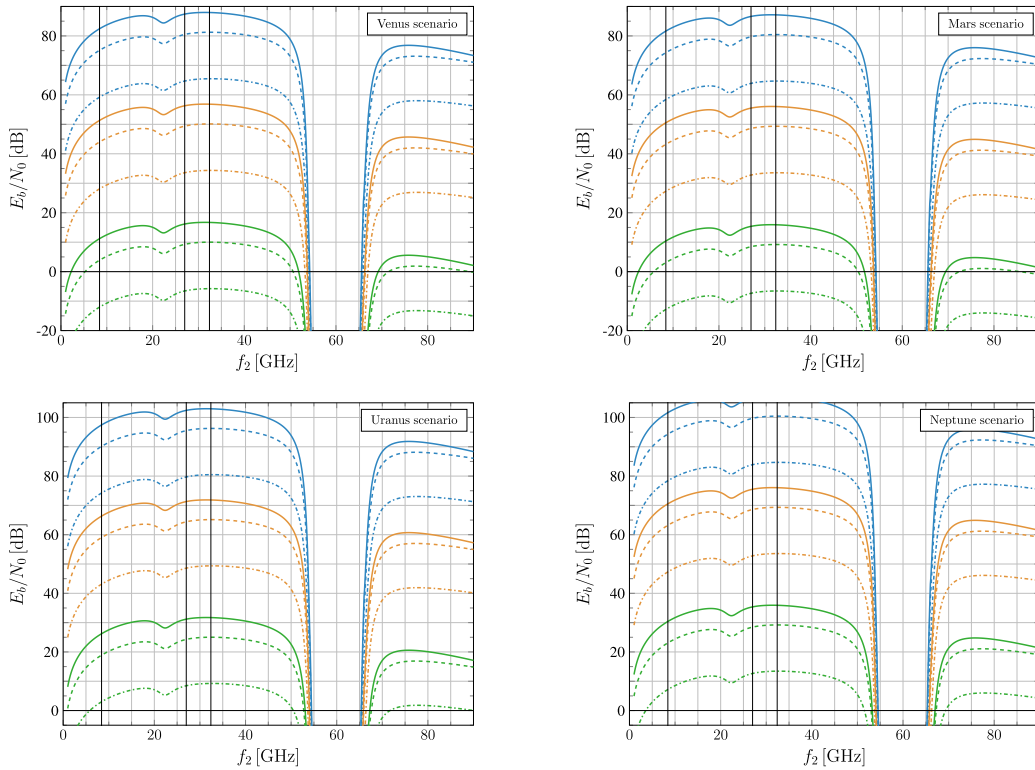
Fig. 4. Available E_b/N_0 values at the G/S for leg-2 in a two-leg system with regenerative relay, versus the leg-2 frequency f_2. Data rates: 100kbps (Venus), 120kbps (Mars), 3.15kbps (Uranus), 1.2kbps (Neptune). Blue: GEO relay; orange: L1 relay; green: L4/L5 relay. Solid: G/S antenna diameter 35m; dashed: G/S antenna diameter 15m; dot-dashed: G/S antenna diameter 2.4m. The black vertical lines correspond to frequencies 8.42, 27, and 32.4 GHz.

the Ka-band allows meeting the 4.23dB requirement even with a G/S antenna diameter of 2.4m. More in detail, the available E_b/N_0 is equal to 9.25dB in the Uranus scenario and to 13.43dB in the Neptune one. This is instead not the case in the Venus and Mars scenarios, where the higher data rate makes the link margin poorer: Considering again the Ka-band and a G/S antenna diameter of 2.4m, we have $E_b/N_0 = -5.77$dB for Venus and $E_b/N_0 = -6.56$dB for Mars. In the Venus and Mars scenarios, we can calculate the minimum G/S antenna size to fulfil the $E_b/N_0 \geq 4.23$ dB requirement assuming $f_2 = 32.4$ GHz, 95% availability and $10°$ elevation. We obtain a G/S antenna diameter of 7.7m for the Venus scenario and of 8.4m for the Mars scenario. These values are remarkably lower that the DSA ones (35m), and are upper bounds to the case of 90% availability and $20°$ elevation often targeted for the Ka-band. Repeating the analysis for the X-band ($f_2 = 8.42$GHz), considering again 95% availability and $10°$ elevation we obtain 15.7m for Venus and 17.2m for Mars.

  2) EHF Leg-1 Analysis: The analysis of leg-1 is carried out by comparing the G/S P_r/N_0 values of a direct X-band link with the $P_{r,1}N_{0,1}$ values characterizing leg-1 in the two-leg system. A GEO relay is considered, although the obtained results remain essentially valid for the other relay options since the leg-1 range has very little sensitivity to the relay position, even in Lagrange points. The input values are the same for both systems (direct link and two-leg) and are the ones summarized in Table I. The system noise

temperature is assumed equal to $T_{syst} = 100$K both in the ground receiver and in the relay receiver. Coherently with the direct link analysis (Section II-C), the implementation losses are equal to 1.5dB in space (deep-space probe transmitter, relay receiver, relay transmitter) and 0.5dB on ground. The X-band atmospheric attenuation impairing the direct link, computed for 95% availability, $10°$ elevation, and the DSA-1 location, is $A_{atm} = 0.5$dB. For both the direct X-band link and the interplanetary leg-1 of the two-leg system, the pointing losses have been estimated using the approach based on θ_{max}; the values $\theta_{max} = 0.1°$, $\theta_{max} = 0.05°$, and $\theta_{max} = 0.01°$ of maximum pointing error have been assumed for S/Cs (deep-space probe in transmission and relay in reception), while $\theta_{max,G/S} = 100$ μrad $\approx 0.0057°$ has been assumed at the G/S.

  The goal is to investigate the value of the frequency f_1 for which the $P_{r,1}/N_{0,1}$ value of the S/C-to-relay link is equal to the P_r/N_0 of the direct X-band link. When this condition is met, using the same modulation and coding techniques, the direct link and leg-1 achieve the same data rate with the same reliability. As addressed above, leg-2 is not a concern; therefore, the data rate is achieved by the whole two-leg system, with G/S antennas smaller than DSA ones.

  In Figs. 5 and 6, the P_r/N_0 values of the direct X-band link are compared with the $P_{r,1}/N_{0,1}$ values of leg-1 in a two-leg system, for f_1 ranging from 1 to 90GHz and for three different values of the relay receiving antenna diameter $d_{r,1}$, namely, 3, 4, and 5m. In particular, Fig. 5 assumes
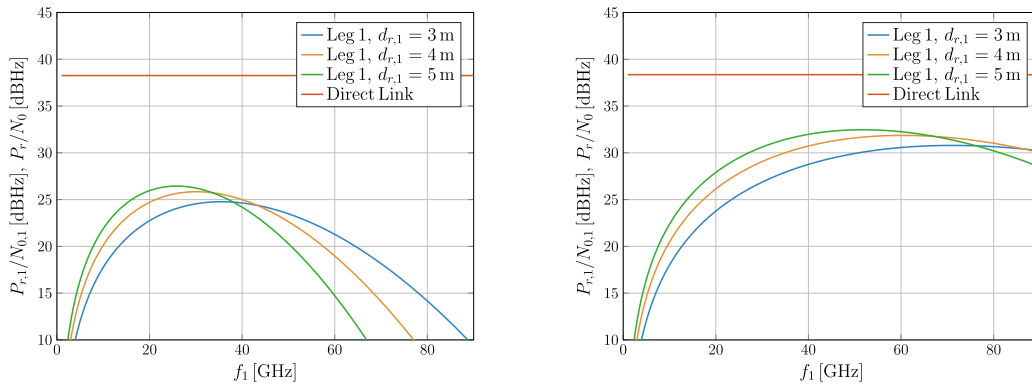
Fig. 5. $P_{r,1}/N_{0,1}$ values of a two-leg system with regenerative relay versus the leg-1 frequency f_1, compared with the P_r/N_0 values of direct link X-band system (red horizontal line); several relay receive antenna diameters; S/C (deep-space and relay) pointing accuracy $\theta_{\max} = 0.1°$ (left) and $\theta_{\max} = 0.05°$ (right); G/S pointing accuracy $\theta_{\max,G/S} = 10^{-4}$rad. Uranus scenario.
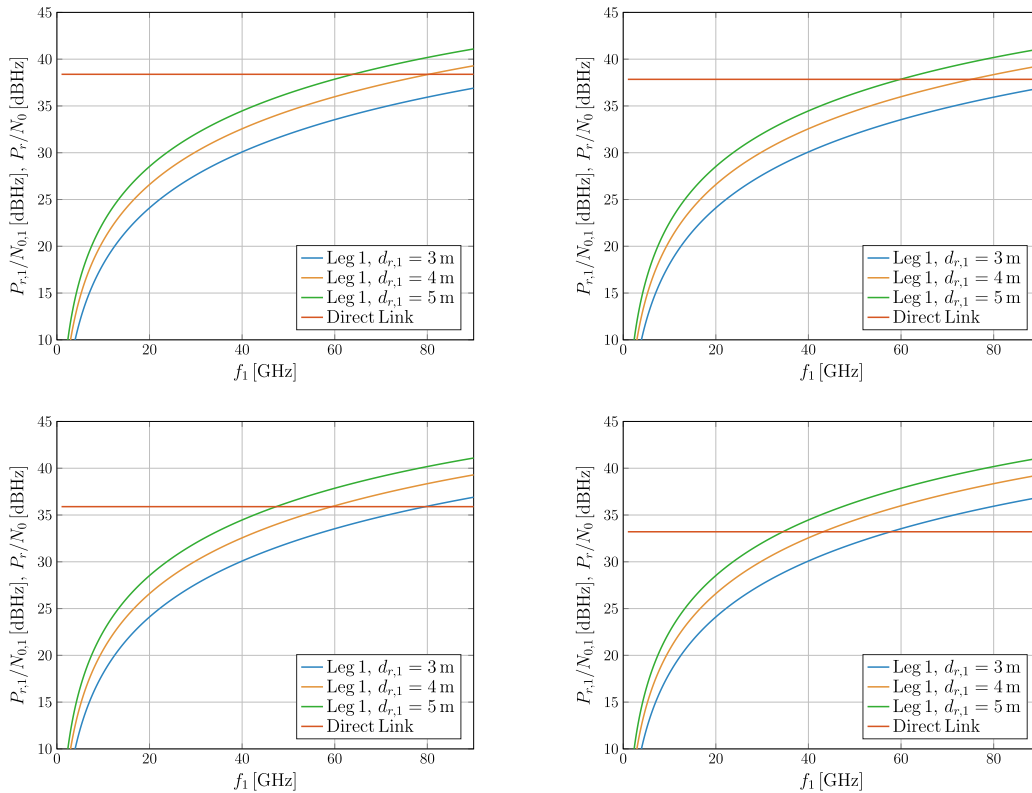

Fig. 6. $P_{r,1}/N_{0,1}$ values of a two-leg system with regenerative relay versus the frequency f_1 in leg 1, compared with the P_r/N_0 values of direct link X-band system (red horizontal line); several relay receive antenna diameters; S/C (deep space and relay) pointing accuracy $\theta_{\max} = 0.01°$ and G/S pointing accuracy $\theta_{\max,G/S} = 10^{-4}$rad. Top-left: 95% availability; top-right: 99% availability; bottom-left: 99.9% availability; bottom-right: 99.99% availability. Uranus scenario.

a maximum pointing error $\theta_{\max} = 0.1°$ and $\theta_{\max} = 0.01°$ in the spacecrafts, while Fig. 6 assumes $\theta_{\max} = 0.01°$. This allows emphasizing the effect of spacecraft pointing errors on the system performance. The considered scenario is Uranus, although results for the other scenarios are very similar and lead essentially to the same conclusions.

As it can be immediately observed from Fig. 5, the two-leg system is outperformed by the X-band direct link one for spacecraft maximum pointing errors $\theta_{\max} = 0.1°$ and $\theta_{\max} = 0.05°$. This is because the $P_{r,1}/N_{0,1}$ value at the

relay receiver is upper bounded by the direct link P_r/N_0 at the G/S over the whole range of frequencies f_1. The situation is different when a better pointing accuracy is met between the deep-space probe and the relay. As shown in Fig. 6, in fact, when $\theta_{\max} = 0.01°$, there exist frequencies f_1, whose values depend on the relay receive antenna diameter, above which leg-1 of the two-leg system outperforms the X-band direct link in terms of $P_{r,1}/N_{0,1}$ compared with the G/S P_r/N_0 of the direct link (hence, in terms of data rate for the same coding, modulation, and reliability requirement).

TABLE VIII
Values of Crossing-Frequency f_1 for Different Availabilities and Different Diameters of the Relay Receiving Antenna

Relay antenna diameter	Availability	Crossing frequency f_1
3.0 m	95.00%	108.3 GHz
	97.00%	105.6 GHz
	99.00%	101.2 GHz
	99.50%	95.4 GHz
	99.90%	79.6 GHz
	99.99%	57.7 GHz
4.0 m	95.00%	80.3 GHz
	97.00%	78.4 GHz
	99.00%	75.2 GHz
	99.50%	71.0 GHz
	99.90%	59.3 GHz
	99.99%	43.2 GHz
5.0 m	95.00%	63.9 GHz
	97.00%	62.4 GHz
	99.00%	59.9 GHz
	99.50%	56.6 GHz
	99.90%	47.4 GHz
	99.99%	34.5 GHz

TABLE IX
Maximum Achievable Ranges, in AU, for Given PPM Order and σ_θ

σ_θ(μrad)	PPM order / peak laser power (W)				
	256 / 1600	64 / 400	32 / 200	16 / 100	4 / 25
1.00	0.113	0.062	0.046	0.034	0.019
0.50	0.453	0.249	0.184	0.136	0.075
0.35	0.924	0.507	0.375	0.277	0.152
0.20	2.836	1.555	1.151	0.851	0.467
0.15	5.037	2.762	2.045	1.512	0.830
0.10	11.342	6.218	4.605	3.406	1.869
0.05	45.350	24.864	18.411	13.617	7.474
B_r (kbps)	32.33	97.00	161.66	258.66	517.32

Results found using Gaussian beam model, $R = 1/3$, $T_s = 256$ns, $n_b = 1.21 \times 10^7$phe/s, $P_{av} = 5$W, $P_{out} = 5\%$, $\lambda = 1064$nm, link margin 3dB.

TABLE X
Maximum Achievable Ranges, in AU, for Given PPM Order and θ_{max}

θ_{max}(μrad)	PPM order / peak laser power (W)				
	256 / 1600	64 / 400	32 / 200	16 / 100	4 / 25
1.00	0.539	0.295	0.219	0.162	0.089
0.50	2.155	1.182	0.875	0.647	0.355
0.35	4.397	2.411	1.785	1.320	0.725
0.20	13.470	7.385	5.468	4.044	2.220
0.15	23.807	13.053	9.665	7.148	3.924
0.10	53.880	29.541	21.874	16.178	8.880
B_r (kbps)	32.33	97.00	161.66	258.66	517.32

Results found using Gaussian beam model, $R = 1/3$, $T_s = 256$ns, $n_b = 1.21 \times 10^7$phe/s, $P_{av} = 5$W, $\lambda = 1064$nm, link margin 3dB.

Fig. 6 also elaborates on the result by varying the percentage of direct X-band link availability, considering 99%, 99.9%, and 99.99%, besides the standard value 95%, the maximum pointing error at the G/S being $\theta_{max,G/S} = 100$ μrad in all cases. As it can be seen, the effect of a higher availability is to reduce the crossover frequency f_1 beyond which leg-1 outperforms the direct link. The values of crossover frequencies f_1 corresponding to the four charts in Fig. 6 are summarized in Table VIII, in which also the availability values 97% and 99.5% have been considered for the sake of completeness. As we can see, a relay receive antenna diameter of 3m can achieve a gain over the direct link system, only for frequencies f_1 that are larger that about 80GHz, unless an unusually high availability of 99.99% is targeted. In contrast, a relay receive antenna diameter of 4m with an f_1 frequency in the range 71–80GHz or a relay receive antenna diameter of 5m with an f_1 frequency in the range 56-64GHz are the minimum requirements for the two-leg system to achieve a gain over the X-band direct one, assuming values of availability ranging between 95 and 99.5%.

3) *Optical Leg-1 Analysis:* We now analyze the case of an optical leg-1. We start by analyzing the maximum range that can be achieved for different values of the pointing accuracy σ_θ (or θ_{max}) and the transmit peak power P_{peak}. Then, a detailed analysis is presented for the specific case of Venus in worst-case range conditions.

The analysis has been carried out using an efficiency equal to -5dB for both the transmit and the receive antennas, a link margin of 3 dB (as in [36]), and supplementary detection and implementation losses equal to -4 dB (as in [37]). The mean background noise flux is set to $n_b = 1.21 \times 10^7$phe/s, the average transmit power to $P_{ave} = 5$W, and the wavelength to $\lambda = 1064$nm. The target leg-1 decoding error probability is set to $P_{e,1}^* = 9 \times 10^{-5}$; using $P_{e,2}^* = 1 \times 10^{-6}$ in leg-2, this choice guarantees a total decoding error probability fulfilling $P_e^* \leq 1 \times 10^{-4}$

(Section IV-B). The outage probability of the system due to mispointing, when the probabilistic approach is used, is set to 5%; moreover, the Gaussian beam model is adopted (worst case) and the transmit and receive antennas are assumed equal in terms of diameter and pointing accuracy. The choice of the numerical value of n_b deserves some explanation. As the maximum achievable range analysis does not refer to a specific scenario (i.e., to a deep-space spacecraft probe a specific planet), a "universal" value of n_b need to be employed. The value $n_b = 1.2 \times 10^7$phe/s has been chosen because it is often suggested in the literature (e.g., [34], together with wavelength $\lambda = 1064$nm) as a "high-noise" condition in deep-space optical links.

Under this setting, we can investigate the maximum achievable range when the most powerful SCPPM configuration [32] is used. This configuration is characterized by $T_s = 256$ns and $R = 1/3$. Tables IX and X report the maximum achievable range values, expressed in astronomic units, for the two different pointing losses estimation approaches (probabilistic and deterministic) and for different choices of the system parameters, such as the PPM order M. For each value of M, the peak transmit power corresponding to an average power $P_{ave} = 5$W is also shown, together with the information bit rate B_r in the bottom line of the table. For a better interpretation of the obtained maximum achievable ranges and for the reader's convenience, we recall that the worst-case ranges of the four considered planets are 1.7AU (Venus), 2.6 AU (Mars), 21.1 AU (Uranus), and 31.3 AU (Neptune). The obtained results reveal how the pointing accuracy requirement is a critical parameter in the optical link design. This is related to the impossibility to achieve

TABLE XI
Example of Venus TM Optical Link Budget With Pointing Losses

Link parameter	dB		Units
Signaling and fixed parameter			
PPM order		64	
Convolutional code rate		1/3	
Slot time		256	ns
Guard time		25	%
Mean noise flux	−3.84	0.413	phe/ns
Mean noise flux per slot		105.63	phe/slot
θ_{max} pointing accuracy, Gaussian beam		0.35	μrad
Laser transmitter			
Average laser power	6.99	5.00	W
Peak laser power	26.02	400	W
Wavelength		1550	nm
Deep space orbiter			
Far-field antenna gain	129.00	1.39	m
Transmitter efficiency	−5.00		
Range			
Space loss	−366.46	1.74	AU
Near earth orbiter			
Receiver gain	129.00	1.39	m
Receiver efficiency	−5.00		
Other			
Detection/implementation losses	−4.00		
Pointing loss	−8.45		
Link performance			
Average received power	−123.93		W
Average received photon flux	−25.00	3.16e−03	phe/ns
Minimum average received power	−127.60		W
Minimum average received photon flux	−28.68	1.36e−03	phe/ns
Link margin	3.67		
FER target		9.00e−05	
Information data rate		0.10	Mbps

Example of Venus TM Optical Link Budget With Pointing Losses on Both the Transmitter and the Receiver, Maximum effective system gain.

unbounded gains when pointing losses are included in the model, as seen in Section IV-C. The pointing accuracy requirement is even more critical when, as in our analysis, pointing losses are included in both the receiver and the transmitter. Overall, we see that sub-μrad level pointing accuracy is required to establish an optical leg-1. A specific analysis is presented next for one of the scenarios of interest.

An accurate optical link budget for leg-1 has been obtained in the Venus scenario, assuming as usual the worst-case range. It is presented in Table XI. Regarding the mean noise flux n_b, its value for this specific scenario has been estimate using the model in [36] as reported in Section IV-D. The link budget shows that a data rate of 100kbps, the same supported by a direct Venus-to-Earth link (Table II), can be supported by leg-1 of a two-leg system with optical technology. Notably, this is possible with an optical antenna size of 1.39m onboard S/Cs (both the deep space one and the relay) and a pointing accuracy of $\theta_{max} = 0.35\mu$rad. When these requirements are met, the two-leg system (including leg-1 and leg-2) achieves the same data rate and reliability and the direct link system, using G/S antenna sizes remarkably lower than DSA ones, as discussed in Section V-B1.

VI. SYSTEM ENGINEERING RESOURCES FOR AN OPTICAL LINK

Given that optical communication in deep space is not yet a mature technology, the impact of implementing such link in leg-1 of a 2-leg data relay architecture needs to be addressed from a system resources perspective. Accordingly, mass/size estimates have been computed both for the deep-space and data relay terminals, although the former is expected to be the one subject to more stringent constraints since the data relay subsystem would not be the primary mission payload. These estimates are then compared to the mass that can be reasonably expected to be dedicated to the communication subsystem onboard the hosting spacecraft.

Following [38], it is possible to allocate the communication subsystem mass as a percentage of the total dry mass depending on the spacecraft type from available historical data. For a planetary exploration spacecraft, this fraction is 6%–7%, and increases to 28% for a communication satellite. The former can be assumed as the reference class for the deep-space terminal, while the latter could be assumed as the reference for the data relay node. Note that a mass fraction of about 28% is also corroborated by a study on a new light-TDRS [39]. In this framework of a two-leg deep-space architecture, however, we cannot assume the entire mass fraction being allocated to data relay on leg-1, since data relay on leg-2 (toward Earth GS) might involve a different band, e.g., Ka. Thus, in this analysis, we conservatively adopt a lower fraction, 20%, for leg-1 data relay subsystem.

Mass estimates for the two terminals are further split according to different assumed S/C size ranges. For the deep-space terminal, light, medium, and heavy classes are considered, which yields to the following mass allocation to the communication subsystem (comm. mass):

1) Light: S/C dry mass = 400–600kg; comm. mass = 24–42kg.
2) Medium: S/C dry mass = 1000–1200kg; comm. mass = 60–84kg.
3) Heavy: S/C dry mass = 2000–2200kg; comm. mass = 120–154kg.

For the data-relay spacecraft, two sizes are considered, which are representative of the current generation TDRS-M spacecraft and of the light-TDRS concept, yielding to

1) TDRS-M: S/C dry mass = 1800kg; comm. mass = 504kg; leg-1 comm. mass = 360kg;
2) Light-TDRS: S/C dry mass = 745kg; comm. mass = 208.6kg, leg-1 comm. mass = 149kg.

A. Engineering Resources for an Optical Link

According to the method in [34], the optical transceiver mass can be expressed as the sum of the following:

1) M_{opt}: mass of the optical head of the telescope, which shows a dependency on the telescope aperture diameter;
2) M_{las}: mass of the transmitter equipment, which shows a dependency on the laser average power.

The empirical equations for computing M_{opt} and M_{las} as a function of the optics diameter and average power are [34]

$$M_{opt}\,[\text{kg}] = K \cdot D^{2.57}$$
$$M_{las}\,[\text{kg}] = 1.152 \cdot P_{opt} + 3.168 \qquad (29)$$

where $K = 0.00181$, D is the telescope diameter in centimeters, and P_{avg} is the laser average power. Allocating the mass for the deep-space optical communication segment according to the above estimates for the three S/C classes, and assuming $P_{avg} = 5W$, the maximum diameters of the optical assembly would be

1) Light: $D = 34{-}{-}42cm$;
2) Medium: $D = 54{-}63cm$;
3) Heavy: $D = 73{-}81cm$.

Following the same logic for the data relay, the equivalent diameters would instead be

1) TDRS-M: $D = 114cm$;
2) Light-TDRS: $D = 80cm$.

In all cases, with the same mass allocation considered for traditional RF communication segments, the maximum diameter achievable for the optical terminal is lower than the optimal diameter estimated in Section V-B3, equal to 139cm. Accordingly, the actual gain would be lower. The difference between optimum diameter and achievable one is smaller for the data relay S/C, and it is reasonable to assume, in this case, a greater engineering effort to accommodate a more performing communication equipment. Although the optical antenna diameter is comparable with the diameter of traditional parabolic dish antennas commonly employed in deep-space missions, the mass associated with the optical diameter is considerably higher than that of traditional RF antennas. This leads to the recommendation of investing in the development of optical antenna designs optimized for reducing the gain/mass ratio.

VII. CONCLUSION

In this article, we analyzed two-leg deep-space relay architectures for assessing their potential advantages over classical direct RF links for data downlink. The problem was tackled from several perspectives. A mathematical framework for analysis of two-leg deep-space relay communication systems was first developed, addressing both the transparent and the regenerative relay cases. In the former case, the EHF band was considered in leg-1 (the interplanetary link), while in the latter case, the analysis included both optical and EHF technologies in leg-1, as well as classical RF frequencies in leg-2. Different two-leg orbital architectures were assessed, assuming the relay to be placed whether on LEO, GEO, or at a Lagrange point of the Earth–Sun system, and the deep-space probe orbiting at an inner or outer planet. The various combinations were then explored in terms of range, complexity, and expected outage periods due to the presence of the Sun in the vicinity of the optical terminals' FOVs. Our results highlighted that two-leg deep-space relay systems, when used with regenerative relays, can provide advantages over direct link systems, provided that specific values of the system parameters can be supported.

The main conclusions may be summarized as follows:

1) A two-leg regenerative relay system with optical frequencies in leg-1 can achieve the same data rates achieved in direct links in the Venus scenario, provided a pointing accuracy of 0.35 μrad can be guaranteed onboard S/Cs (deep-space probe and relay), together with an average transmit power of 5W, a peak transmit power of 400W, and an optical antenna size in the order of 1.4m.
Although a detailed optical link budget was shown in Section V-B3 only for the Venus case, the analysis can be repeated for the other scenarios. In the Mars case, we obtained the same parameters and pointing requirement. Regarding Uranus and Neptune, more tightening pointing accuracy constraints have been obtained, as low as 0.1 μrad, together with an average transmit power of 5W, a peak transmit power of 400W, and an optical antenna size of about 5m.
2) Two-leg regenerative relay systems operating in EHF band in leg-1 can achieve the same data rates achieved in direct links, provided a pointing accuracy of 0.01° can be guaranteed onboard S/Cs (in all scenarios), with a leg-1 frequency $f_1 \approx 64$ GHz, and an antenna size in the order of 5m.
3) In both cases (optical and EHF), due to the large margin available in leg-2, antenna sizes smaller than the typical DSA ones can be used on ground. For a GEO relay, antenna diameters of 2.4m (corresponding, for example, to ESA REDU-3) can be employed in all scenarios with a frequency $f_2 = 27$GHz. For a Lagrange L4/L5 relay and a Ka-band relay-to-ground link, antenna diameters of 2.4m can be employed in the Uranus and Neptune scenarios, while larger antenna sizes, yet smaller than DSA ones, are necessary in the Venus and Mars ones due to the higher data rate. For example, with a concatenated coding scheme, diameters in the order of 7.7 and 8.4m are necessary for the Venus and Mars scenarios, respectively.
4) In both cases (optical and EHF), the two-leg system bottleneck is represented by leg-1. This is mainly due to pointing losses severely affecting both the transmitter and the receiver. In contrast, the available analyses for direct link systems, RF or optical, include pointing losses on the spacecraft side but not on the ground side.
5) In case of optical frequencies, different planetary targets may lead to different expected mission coverage in downlink, depending on the assumed minimum offset angle the optical terminal is designed to operate at. Stringent design constraints are expected on the optical terminal of a deep-space probe at Uranus or Neptune, as it must be capable to operate at an SPD angle always smaller than 0.5°.

TABLE XII
Summary of Link Analysis

Configuration	Direct link	Two-leg Optical leg-1	Two-leg EHF leg-1
Tx power	65 W	5 W (average) 400 W (peak)	65 W
Leg-1 band	8.42 GHz	1550 nm	63.9 GHz
Leg-2 band	–	27 GHz (GEO/L1) 32.4 GHz (L4/L5)	27 GHz (GEO/L1) 32.4 GHz (L4/L5)
Relay Rx antenna	–	1.39 m	5 m
Venus (V) – 1.73 AU			
Deep space S/C antenna	1.3 m	1.39 m	1.3 m
Data rate	100 kbps	100 kbps	100 kbps
S/C pointing accuracy	0.05°	0.35 µrad	0.01°
Mars (M) – 2.68 AU			
Deep space S/C antenna	2.2 m	1.39 m	2.2 m
Data rate	120 kbps	100 kbps	120 kbps
S/C pointing accuracy	0.05°	0.35 µrad	0.01°
Uranus (U) – 21.1 AU			
Deep space S/C antenna	3 m	5 m	3 m
Data rate	3.15 kbps	100 kbps	3.15 kbps
S/C pointing accuracy	0.05°	0.1 µrad	0.01°
Neptune (N) – 31.3 AU			
Deep space S/C antenna	3 m	5 m	3 m
Data rate	1.20 kbps	100 kbps	1.20 kbps
S/C pointing accuracy	0.05°	0.1 µrad	0.01°
Ground antenna	35 m	2.4 m (GEO/L1–all) 7.7 m (L4/L5–all)	2.4 m (GEO/L1–all) 2.4 m (L4/L5–U/N) 7.7 m (L4/L5–V) 8.4 m (L4/L5–M)

6) A two-leg architecture with a relay spacecraft in L4/L5 would take advantage of a larger angular separation from the Earth, so that when either L4 or L5 is at low SDP angles, ground-based deep-space antennas on the Earth may be used to send telecommands to the deep-space probe, thereby virtually eliminating any outage due to occultations.

7) With the same mass allocation considered for traditional RF communication segments, the maximum diameter obtainable for the optical terminal onboard the deep-space spacecraft is smaller than that required by the optimal effective system gain. It is thus recommended to seek for novel optical antenna designs featuring increased gain/mass ratios.

A summary of the most significant link analysis results is shown in Table XII, for the regenerative relay case. In the table, the two-leg architecture based on EHF in leg-1 is compared with a direct X-band link for the same information bit rate. In the case of optical technology used in leg-1, instead, the SCPPM parameters $M = 64$, $R = 1/3$, and $T_s = 256$ns are the same in all scenarios, resulting in the same data rate. These parameters are addressed in the Appendix.

Since both optical and EHF technologies can guarantee similar advantages in leg-1, the choice of the system architecture is mainly dictated by the capability of current systems to support the above-mentioned set of parameters; out of them, the most critical ones seem to be represented by the required pointing accuracy levels in the optical case and by the relay receive antenna size in the RF one. The choice of the specific leg-1 technology may change depending on the scenario. For example, should the optical pointing requirement for Mars and Venus be feasible, while the one for Uranus and Neptune be too tight, an optical system may be chosen in the former scenarios and an RF one for the latter ones.

We close the article by pointing out that the use of the optical technology in leg-2 has not been addressed in this work for several reasons, including 1) the significant impact of the atmospheric effects, potentially quite severe especially at low elevation angles; 2) problems arising in the spacecraft pointing accuracy, as an optical uplink beacon would be significantly affected (much more than the downlink) by scintillation and beam wandering, again due to the Earth atmosphere; 3) the fact that the technology for L4/L5-to-ground optical links is not as mature and consolidated as it is for intersatellite links or as the RF one [40]. It is, however, undoubted that the technological development of optical communications is currently gaining a momentum, as witnessed by the intensified standardization activities within the Consultative Committee for Space Data Systems (CCSDS) and by a set of in-orbit demonstrators and missions from several space agencies, including ESA HydRON [41], NASA TBIRD [42], and DLR Osiris [43]. The analysis of RF-optical or optical-optical two-leg deep-space relay systems is therefore an important challenging direction of further investigation.

TABLE XIII
Input Block Sizes for the Three Possible SCPPM Code Rates

Convolutional code rate	Information block size (bits)	Input block size to SCPPM encoder (bits)
1/3	5006	5040
1/2	7526	7560
2/3	10046	10080

APPENDIX A
SCPPM CODED MODULATION

The SCPPM-encoding scheme accepts as input information blocks with configurable size and generates a sequence of coded PPM symbols which form an SCPPM codeword [32], [44]. Depending on the chosen code rate of the convolutional encoder, whose admitted values are 1/3, 1/2, and 2/3, the information bits are sliced into blocks whose sizes are reported in Table XIII. A 32-bit CRC code, used for block error detection, is attached to each information block. Then, before the block is passed to the SCPPM encoder, two 0 bits are appended to it (termination bits) in order to let the convolutional encoder terminate in the zero state before the next block is processed. The input block so generated is denoted by $\boldsymbol{u}$. Its admitted sizes are shown in the third column of Table XIII.

The SCPPM encoder is composed of an outer convolutional encoder, a bit interleaver, and an accumulator-PPM (APPM) referred to as the "inner encoder." The convolutional encoder is described by the generator polynomials

$$g^{(1)}(D) = 1 + D^2$$
$$g^{(2)}(D) = 1 + D + D^2$$
$$g^{(3)}(D) = 1 + D + D^2 \tag{30}$$

along with the puncturing patterns specified in [32]. The three code rates require three different lengths for the input block $\boldsymbol{u}$, as previously described, to generate a fixed-length output of 15 120 bit. The advantage of adopting a fixed length output (i.e., coded) block is the possibility to implement a single interleaver, specified by the function

$$\pi(j) = 11j + 210j^2 \bmod 15120 \tag{31}$$

where j is the index of the input bit and $\pi(j)$ is the corresponding output index. The scrambled bits are then processed by the APPM (inner encoder). The bits are first processed by a rate-1 accumulator and then they are divided into sub-blocks of $m = \log_2 M$ bit each, where M is the PPM order, $M \in \{4, 8, 16, 32, 64, 128, 256\}$. Each sub-block of m bits is mapped onto a PPM symbol, yielding $15120/\log_2 M$ PPM symbols per input block. A Gray or anti-Gray bit mapper may be introduced between slicing into sub-blocks and PPM modulation. The SCPPM standard also imposes a 25% guard time between the PPM symbols, where an M-PPM symbol is represented as a sequence of M time slots, of which only one is pulsed (the pulsed slot depends on the value of the corresponding m bits). Typical values for the slot time T_s are in the range 0.5–256ns. Hence,
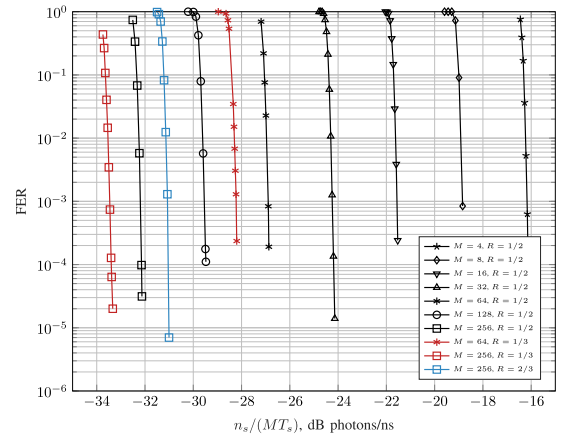

Fig. 7. Frame error rate of SCPPM codes assuming $n_b = 0.2$ phe/slot, $T_s = 16$ ns, and Gray mapping.

each PPM symbol has a time duration equal to MT_s; the guard time duration is $MT_s/4$.

An efficient turbo-like iterative decoding scheme can be used to decode SCPPM codes. This scheme, based on two soft-input soft-output module exchanging information in an iterative fashion, allows achieving a performance that approaches the one obtained by optimum maximum a posteriori decoding. A "logical" M-PPM symbol can be thought as a vector of size M in which all elements are null except one element, corresponding to the pulsed slot, which is equal to one. When this symbol is transmitted by a laser system, we can represent the received symbol as a vector $\boldsymbol{y}$, again of size M, each element of which is a nonnegative integer representing the number of photo-detected photons. Considering a Poisson PPM channel, a typical optical channel model, the conditional probabilities to detect k photons in a given slot, conditioned to the slot being empty ("0") or pulsed ("1"), are given by

$$p_{Y|C}(k|1) = \frac{(n_s + n_b)^k \, e^{-(n_s + n_b)}}{k!} \tag{32}$$

$$p_{Y|C}(k|0) = \frac{n_b^k e^{-n_b}}{k!} \tag{33}$$

where n_b is the average number of noise photons per slot and n_s is the average number of received signal photons in a pulsed slot.

Fig. 7 shows the performance of SCPPM codes simulated with different values of the PPM order M and code rate; all curves are relevant to a slot time $T_s = 16$ ns, $n_b = 0.2$ phe/slot, and 25 decoding iterations per codeword. As we can observe, for given T_s, n_b, and convolutional code rate, the larger is the PPM order and the better is the SCPPM performance; the scheme, in fact, requires a smaller average number of signal photons per nanosecond to achieve a target FER. Interestingly, the gap between different simulated curves exhibits an almost systematic behavior. More specifically, doubling M turns into a coding gain of approximately 2.5 dB. Our simulations also confirm that, as expected, for a given order M, the SCPPM scheme with code rate 1/3 (red curves, for $M = 64$ and $M = 256$) achieves the best performance, followed by the one with code rate 1/2 (black

curves) and finally by the one with code rate 2/3 (blue curve for $M = 256$).

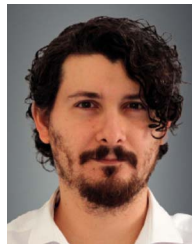## ACKNOWLEDGMENT

REFERENCES

[1]   R. A. Stampfl and A. E. Jones
        Tracking and data relay satellites
        IEEE Trans. Aerosp. Electron. Syst., vol. AES-6, no. 3,
        pp. 276–289, May 1970.

[2]   B. Kopp, J. Harris, and C. Lauand
        Utilizing existing commercial geostationary Earth orbit fixed
        satellite services for low earth orbit satellite communication
        relays with earth
        New Space, vol. 7, no. 1, pp. 19–30, 2019.

[3]   K. Hogie, E. Criscuolo, A. Dissanayake, B. Flanders, H. Safavi,
        and J. Lubelczyk
        TDRSS demand access system augmentation
        In *Proc. IEEE Aerosp. Conf.*, Big Sky, MT, USA, 2015,
        pp. 1–10.

[4]   M. Witting
        et al. Status of the European data relay satellite system
        In *Proc. Int. Conf. Space Opt. Syst. Appl.*, Ajaccio, France, 2012,
        pp. 19–30.

[5]   J. Hunter
        The orbiting deep space relay station – A study report
        In *Proc. AIAA Conf. Large Space Platforms: Future Needs
        Capabilities*, Los Angeles, CA, USA, 1978, Art. no. 1639.

[6]   K. E. Wilson
        et al. Cost and performance comparison of an Earth-orbiting
        optical communication relay transceiver and a ground-based
        optical receiver subnet
        IPN Progress Rep. 42-153, Jan.–Mar. 2003, pp. 1–12.

[7]   M. Wittig
        Data relay for Earth, Moon and Mars missions
        In *Proc IEEE Int. Workshop Satell. Space Commun.*, 2009,
        pp. 300–304.

[8]   H. Hemmati, A. Biswas, and I. B. Djordjevic
        Deep-space optical communications: Future perspectives and
        applications
        Proc. IEEE, vol. 99, no. 11, pp. 2020–2039, Nov. 2011.

[9]   R. Cesarone, D. Abraham, S. Shambayati, and J. Rush
        Deep-space optical communications: Visions, trends, and
        prospects
        In *Proc. IEEE Int. Conf. Space Opt. Syst. Appl.*, Santa Monica,
        CA, USA, 2011, pp. 410–423.

[10]   D. M. Cornwell
        NASA's optical communications program for 2017 and beyond
        In *Proc. IEEE Int. Conf. Space Opt. Syst. Appl.*, 2017, pp. 10–14.

[11]   W. Hurd *et al.*
        Exo-atmospheric telescopes for deep space optical communi-
        cations
        In *Proc. IEEE Aerosp. Conf.*, Big Sky, MT, USA, 2006,
        pp. 1–12.

[12]   L. Valentini, A. Faedi, E. Paolini, and M. Chiani
        Analysis of pointing loss effects in deep space optical links
        In *Proc. IEEE Glob. Commun. Conf.*, Madrid, Spain, 2021,
        pp. 1–6.

[13]   *Propagation Data and Prediction Methods Required for the Design
        of Earth-Space Telecommunication Systems*, ITU-R P.618-13,
        International Telecommunication Union - Radiocommunica-
        tion Sector Standard, Dec. 2017.

[14]   *Attenuation by Atmospheric Gases and Related Effects*, ITU-R
        P.676-12, International Telecommunication Union - Radiocom-
        munication Sector Standard, Aug. 2019.

[15]   *Attenuation due to Clouds and Fog*, ITU-R P.840-8, International
        Telecommunication Union - Radiocommunication Sector Stan-
        dard, Aug. 2019.

[16]   J. J. Rivera *et al.*
        Alphasat Aldo Paraboni, an advanced Q/V band mission space
        segment
        Int. J. Satell. Commun. Netw., vol. 37, no. 5, pp. 397–409, 2019.

[17]   X. Boulanger and L. Castanet
        Ka and Q band propagation experiments in Toulouse using
        ASTRA 3B and ALPHASAT satellites
        Int. J. Satell. Commun. Netw., vol. 37, no. 5, pp. 449–459, 2019.

[18]   C. Riva *et al.*
        The Alphasat Aldo Paraboni propagation experiment: Measure-
        ment campaign at the Italian ground stations
        Int. J. Satell. Commun. Netw., vol. 37, no. 5, pp. 423–436, 2019.

[19]   A. Kelmendi, A. Hrovat, M. Mohorčič, and A. Švigelj
        Alphasat propagation measurements at Ka- and Q- bands in
        Ljubljana: Three years' statistical analysis
        IEEE Antennas Wireless Propag. Lett., vol. 20, no. 2,
        pp. 174–178, Feb. 2021.

[20]   F. Cuervo, J. Ebert, M. Schmidt, and P.-D. Arapoglou
        Q-band LEO Earth observation data downlink: Radiowave
        propagation and system performance
        IEEE Access, vol. 9, pp. 165611–165617, 2021.

[21]   *Space Engineering — Radio Frequency and Modulation*, ECSS-E-
        ST-50-05C Rev. 2, European Cooperation for Space Standard-
        ization Standard, Oct. 2011.

[22]   M. Shihabi, T. M. Nguyen, and S. Hinedi
        A comparison of telemetry signals in the presence and absence
        of a subcarrier
        IEEE Trans. Electromagn. Compat., vol. 36, no. 1, pp. 60–73,
        Feb. 1994.

[23]   P. Müller
        ESA tracking stations (ESTRACK) facilities manual (EFM)
        DOPS-ESTR-OPS-MAN-1001-OPS-ONN
        Sep. 2008.

[24]   P. Besso
        Present and future feed systems for ESA deep space antennas
        In *Proc. Int. Conf. Electromagnetics Adv. Appl.*, Turin, Italy,
        2015, pp. 12–15.

[25]   E. Matricciani
        Deep-space communications with a 2-Hop downlink with high
        link-availability
        Int. J. Satell. Commun., vol. 23, no. 4, pp. 203–228, Jul. 2005.

[26]   E. Matricciani
        An optimum design of deep-space downlinks affected by tro-
        pospheric attenuation
        Int. J. Satell. Commun., vol. 27, no. 6, pp. 312–319,
        Nov./Dec. 2009.

[27]   M. O. Hasna and M.-S. Alouini
        Outage probability of multihop transmission over Nakagami
        fading channels
        IEEE Commun. Lett., vol. 7, no. 5, pp. 216–218, May 2003.

[28]   C.-C. Chen and C. S. Gardner
        Impact of random pointing and tracking errors on the design of
        coherent and incoherent optical intersatellite communication
        links
        IEEE Trans. Commun., vol. 37, no. 3, pp. 252–260, Mar. 1989.

[29]   V. Vilnrotter
        The effects of pointing errors on the performance of optical
        communications systems
        TDA Prog. Rep. 42, vol. 63, pp. 136–146, 1981.

[30]   J. Barry and G. Mecherle
        Beam pointing error as a significant design parameter for
        satellite-borne, free-space optical communication systems
        Opt. Eng., vol. 24, no. 6, 1985, Art. no. 241049.

[31]   S. J. Orfanidis
        Electromagnetic waves and antennas
        2008. [Online]. Available: available: http://www.ece.rutgers.
        edu/orfanidi/ewa

[32] *Optical Communications Coding and Synchronization*, Blue Book 142.0-B-1, Consultative Committee for Space Data Systems Standard, Aug. 2019.

[33] A. Biswas and S. Piazzolla
Deep-space optical communications downlink budget from Mars: System parameters
IPN Prog. Rep., 42-154, Nov. 2003.

[34] A. Biswas, H. Hemmati, B. M. S. Piazzolla, K. Birnbaum, and K. Quirk
Deep-space optical terminals (DOT) systems engineering
IPN Prog. Rep. 42-183, Nov. 2010, pp. 1–12.

[35] R. M. Gagliardi and S. Karp
Optical Communications. New York, NY, USA: Wiley, 1976.

[36] *Technical and Operational Characteristics of Interplanetary and Deep-Space Systems Operating in the Space-to-Earth Direction Around 283 THz*, Rec. ITU-R SA.1742, International Telecommunication Union - Radiocommunication Sector Standard, Mar. 2006.

[37] A. Biswas, H. Hemmati, S. Piazzolla, B. Moision, K. Birnbaum, and K. Quirk
Deep-space optical terminals (DOT) systems engineering
IPN Prog. Rep., vol. 42, 2010, Art. no. 183.

[38] C. D. Brown
System Engineering
In *Elements of Spacecraft Design*. Reston, VA, USA: American Institute of Aeronautics and Astronautics, Jan. 2002, ch. 2, pp. 19–36.

[39] K. B. Bhasin, S. R. Oleson, J. D. Warner, and J. Schier
Design concepts for a small space-based GEO satellite for missions between low Earth and near Earth orbits
In *Proc. AIAA Space Operations Conf.*, Pasadena, CA, USA, 2014, Art. no. 1688.

[40] Z. Sodnik *et al.*
Deep-space optical communication system (DOCS) for ESA's space weather mission to Lagrange orbit L5
In *Proc. IEEE Int. Conf. Space Opt. Syst. Appl.*, Naha, Japan, 2017, pp. 28–33.

[41] J. Perdigues *et al.*
HYDRON: The ESA initiative towards optical networking in space
In *Proc. Eur. Conf. Opt. Commun.*, Bordeaux, France, 2021, pp. 1–4.

[42] C. M. Schieler, A. S. Garg, B. C. Bilyeu, J. P. Wang, and B. S. Robinson
Demonstration of reliable high-rate optical communication over an atmospheric link using ARQ
In *Proc. IEEE Int. Conf. Space Opt. Syst. Appl.*, Portland, OR, USA, 2019, pp. 1–6.

[43] C. Fuchs and C. Schmidt
Update on DLR's OSIRIS program
In *Proc. SPIE Int. Conf. Space Opt.*, vol. 11180, Chania, Greece, 2018, pp. 192–200.

[44] B. Moision and J. Hamkins
Coded modulation for the deep-space optical channel: Serially concatenated pulse-position modulation
IPN Prog. Rep., 42-161, pp. 1–25, May 2005.

Alfredo Locarini received the Ph.D. degree in mechanics and advanced engineering sciences from the University of Bologna, Bologna, Italy, in 2018.

Since 2018, he has been a Postdoctoral Research Fellow and Lecturer in space systems with the University of Bologna. His research interests include LEO GNSS navigation, small satellites subsystems, and missions analysis.

Lorenzo Valentini (Student Member, IEEE) received the B.S. degree (Summa Cum Laude) in electronics engineering, in 2017, and the M.S. degree (Summa Cum Laude) in electronics and telecommunications engineering, 2019, from the University of Bologna, Bologna, Italy, where he is currently working toward the Ph.D. degree in electronics, telecommunications, and information technologies engineering.

From 2019 to 2020, he was with the Interdepartmental Centre for Industrial ICT Research, University of Bologna, working on Internet of Things. His research interests include communication theory, wireless sensor networks, massive multiple access protocols, and quantum information.

Alberto Faedi received the B.S. degree in electronics engineering and the M.S. degree in electronics and telecommunications engineering from the University of Bologna, Bologna, Italy, in 2017 and 2021, respectively.

From 2021 to 2022, he was with the National Laboratory of Wireless Communications of CNIT (WiLab), University of Bologna, working on massive multiple access for 6G. He is currently an Embedded Software Engineer with Zapi Group, Poviglio, Italy.

Paolo Tortora (Senior Member, IEEE) received the Ph.D. degree in aerospace engineering from the University of Rome "Sapienza", Rome, Italy, in 2001.

He has been with the University of Bologna as an Assistant Professor since 2002, Associate Professor since 2006, and a Full Professor since 2017. He is currently the Director of the Interdepartmental Center for Industrial Research in Aerospace, Capua, Italy. He was the Course Director of the B.Sc. and M.Sc. degrees in aerospace Engineering with the University of Bologna, from 2012 to 2018. His research interests include small satellites and innovative spacecraft subsystems, including the ground segment, and planetary exploration focusing on radio science experiments with deep-space missions.

Dario Modenini (Member, IEEE) received the Ph.D. degree in mechanics and advanced engineering sciences from the University of Bologna, Bologna, Italy, in 2012.

Since 2020, he has been a Senior Assistant Professor in aerospace systems with the University of Bologna. His research interests include small satellites subsystems, spacecraft attitude determination and control, spacecraft navigation, and mission analysis.

Davide Rovelli received the Master's degree in telecommunication engineering from Politecnico di Milano, Milano, Italy, in 2007.

In 2006, he was with Thales Alenia Space, where he worked on GNSS receivers and on the Telemetry Tracking & Control (TT&C) subsystem of deep-space satellites. Since 2019, he has been a TT&C engineer with European Space Agency, Paris, France, supporting various technology developments as well as exploration and science missions.

Nicolò Mazzali (Member, IEEE) received the Ph.D. degree in information technologies from the University of Parma, Parma, Italy, in 2013.

Since 2018, he has been a Communication Systems and Technologies Engineer with the Directorate of Technology, Engineering, and Quality (TEC), European Space Agency (ESA), Paris, France. His research interests include signal processing for satellite communications, synchronization, and estimation theory.

Enrico Paolini (Senior Member, IEEE) received the Ph.D. degree in electrical engineering from the University of Bologna, Bologna, Italy, in 2007.

He was visiting Research Scholar with the University of Hawai'i at Manoa, Honolulu, HI, USA. Since 2015, he has been an Associate Professor with the University of Bologna. His research interests include space and terrestrial communication systems, information theory, error-correcting codes, and detection and tracking in radar systems.

Dr. Paolini was an Editor of the IEEE COMMUNICATIONS LETTERS from 2012 to 2015 and an Editor of the IEEE TRANSACTIONS ON COMMUNICATIONS from 2015 to 2020.

Marco Chiani (Fellow, IEEE) received the Dr. Ing. degree (Summa Cum Laude) in electronic engineering and the Ph.D. degree in electronic and computer engineering from the University of Bologna, Bologna, Italy, in 1989 and 1993, respectively.

He is a Full Professor of Telecommunications with the University of Bologna. Since 2003, he has been a frequent Visitor with the Massachusetts Institute of Technology (MIT), Cambridge, MA, USA, where he currently holds a Research Affiliate appointment. His research interests include information theory, wireless systems, statistical signal processing, and quantum information.

Dr. Chiani was an elected Chair of the Radio Communications Committee of the IEEE Communication Society, from 2002 to 2004, and an Editor of *Wireless Communication* for the IEEE TRANSACTIONS ON COMMUNICATIONS, from 2000 to 2007.